Direct Flux Vector Control of Synchronous Motor Drives: Accurate Decoupled Control with Online Adaptive MTPA and MTPV Evaluation

Direct Flux Vector Control of Synchronous Motor Drives: Accurate Decoupled Control with Online Adaptive MTPA and MTPV Evaluation

Anantaram Varatharajan, *Student Member*, Gianmario Pellegrino, *Senior Member*, and Eric Armando, *Senior Member*

***Abstract*—Direct flux vector control (DFVC) has an unique advantage in facilitating flux-weakening operation due to the choice of controlled variables: stator flux linkage magnitude and torque producing current. However, the dynamics in stator flux oriented reference frame is heavily affected by the nonlinear cross-coupling between the two axes. This paper presents a nonlinear transformation method to decouple the axes for a uniform bandwidth at all operating points. Respect to the literature, the proposed transformation takes magnetic saturation into account without approximation. Furthermore, the auxiliary-flux and auxiliary-current vectors are introduced to design a new adaptive evaluation of maximum torque per ampere (MTPA) and maximum torque per volt (MTPV) control laws, enabling to track the optimal control laws without the need for pre-processed look-up-tables (LUTs). The proposed scheme is experimentally validated on a 1.1 kW synchronous reluctance (SyR) machine test bench.**

***Index Terms*—Direct flux vector control, synchronous machines, flux-weakening, online adaptive reference.**

I. Introduction

Synchronous machines, particularly those with interior permanent magnets, possess high torque density and good flux-weakening capability for extended speed-range. The large constant-power speed range finds importance in a variety of applications such as traction, industrial applications and home appliances. The optimal torque control incorporates maximum torque per ampere (MTPA) and maximum torque per volts (MTPV) criteria and abides the current and voltage constraints at all operating points.

The vast majority of torque control methods are based on current vector control (CVC) schemes, implemented in the rotor synchronous dq coordinates with linear current regulators. The dynamic coupling between d and q axes can be feed-forward compensated and the effect of saturation on the control stability and performance is often regarded as a minor issue. The commanded torque and the operating speed determine the reference current $\boldsymbol{i}^*_{dq}$, fetched from pre-processed lookup tables (LUTs) [1]–[3]. A voltage feedback regulator is designed to regulate flux-weakening at high speeds in [4]–[6]. Alternatively, a gradient descent method is used to track the constant torque locus at high speeds in [7].

Alternative to CVC, direct torque control (DTC) is a prominent technique adopted for its fast dynamic performance and robustness. The direct of control of stator flux linkage inherently facilitates the flux-weakening operations [8] [9]. Similar to DTC in principle, the direct flux vector control (DFVC) has constant switching frequency and straightforward current limitation [10]–[12], thus combining the merits of CVC and DTC. DFVC is implemented in the stator flux oriented reference frame, with the stator flux linkage magnitude λ and the quadrature torque producing current i_τ as the controlled variables. Conventionally, two proportional-integral (PI) regulators are used for the control loops. However, the torque producing current loop is nonlinear and therefore, for constant-gain PI, the dynamics becomes a function of the operating point. A nonlinear transformation matrix is proposed in [13] to decouple and achieve uniform bandwidth of the control loops. However, the effect of magnetic saturation on the nonlinear transformation was overlooked. A model-based DFVC scheme is reported in [14], but it suffers of a similar approximation, besides being noisy under parameters detuning. A deadbeat DFVC is investigated in [15], [16] but the effects of saturation are overlooked.

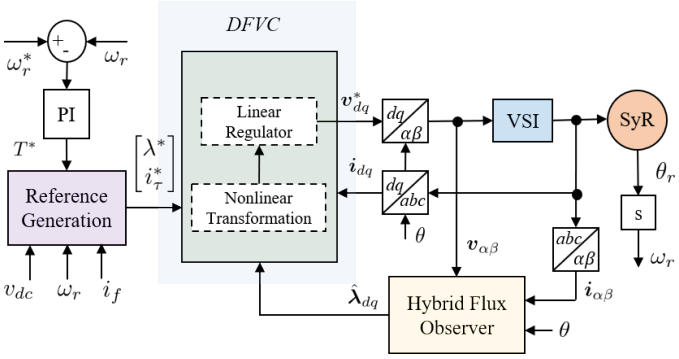

Fig. 1. Overview of control system illustrating the DFVC scheme with nonlinear transformation, hybrid flux observer and optimal reference generation.

Manuscript received Month xx, 2xxx; revised Month xx, xxxx; accepted Month x, xxxx. This work was supported by the Power Electronics Innovation Center (PEIC) of Politecnico di Torino, Italy.

A. Varatharajan, G. Pellegrino and E. Armando are with the Department of Energy, Politecnico di Torino, Turin 10129, Italy. (email: anantaram.varatharajan@polito.it; gianmario.pellegrino@polito.it; eric.armando@polito.it). Corresponding author: Anantaram Varatharajan.

With [13] as the state-of-art, this paper models the nonlinear dynamics of DFVC with improved accuracy taking saturation into account, resulting in a constant control bandwidth and improved resilience to parameter detuning.

The second contribution of this paper regards the online adaptation of the MTPA and MTPV control trajectories. In the literature, the reported works on DFVC use offline preprocessed MTPA and MTPV LUTs computed from the flux-map LUTs of the machine under test. Experimental identification of such flux-map with a dedicated test-bench is reported in [17]. Alternatively, several self-commissioning techniques have been proposed [18]–[20]. The paper proposes an online optimal reference adaptation scheme for LUT-less tracking of the MTPA and MTPV laws, based on the suitably defined auxiliary-flux and auxiliary-current vectors. The adaptive scheme avoids the need for preprocessed reference LUTs, making the control insensitive to MTPA and MTPV variations due to, for example, the temperature effect on permanent magnets.

The main contributions of the paper are enumerated as follows:

1) The modelling of dynamics in stator flux oriented reference frame in Section III is improved over the state-of-art modelling with the inclusion of magnetic saturation.
2) The nonlinear transformation for decoupled DFVC scheme to obtain uniform bandwidth at all operating points is developed in Section IV.
3) The real-time adaptive reference generations is proposed in Section V for operation without preprocessed MTPA and MTPV LUTs.

Section VI presents the experimental validation of the proposed scheme on a 1.1 kW synchronous reluctance (SyR) machine test bench and Section VII concludes the paper.

II. Synchronous Machine Model

The electrical rotor position is θ and the electrical angular speed is $\omega = s\,\theta$ where s is the differential operator $\frac{\mathrm{d}}{\mathrm{d}t}$. Estimated vectors are represented by the superscript $\hat{}$. The orthogonal rotational matrix is $\mathbf{J} = \left[\begin{smallmatrix} 0 & -1 \\ 1 & 0 \end{smallmatrix}\right]$ and $\mathbf{I}$ is the identity matrix.

Real space vectors will be used; for example, the stator current is $\boldsymbol{i}_{dq} = [i_d, i_q]^{\mathrm{T}}$ where i_d and i_q are the vector components in rotor reference frame. Space vectors in the stationary reference frame are denoted by subscript $\alpha\beta$. Note that the convention of a SyR machine is followed, i.e, d-axis is defined along the maximum inductance path. Magnets, if any, are along the negative q-axis. The stator flux reference frame is denoted by the subscript $f\tau$. An overview of the DFVC control system is shown in the Fig. 1. The Fig. 2 illustrates the symbols and notations of the two reference frames.

A. Mathematical Model in dq Reference Frame

The voltage equation of a synchronous machine in rotor reference frame is expressed as

$$s\,\boldsymbol{\lambda}_{dq} = \boldsymbol{v}_{dq} - R_s \boldsymbol{i}_{dq} - \omega\,\mathbf{J}\,\boldsymbol{\lambda}_{dq} \tag{1}$$

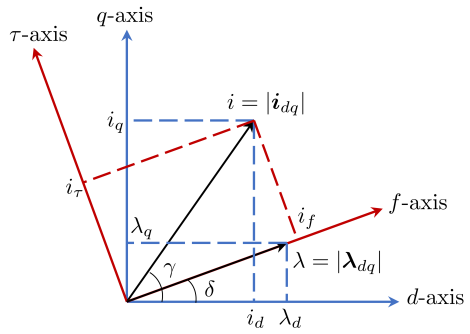

Fig. 2. Illustration of symbols and notations in the dq rotor and $f\tau$ stator flux oriented reference frames.

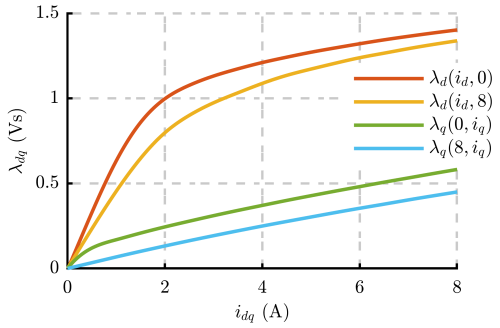

Fig. 3. Flux map of the SyR motor under test. Experimentally identified with the constant speed test, reported in [17].

where R_s is the stator resistance and $\boldsymbol{\lambda}_{dq}$ is the stator flux linkage. The incremental inductance is defined as

$$\boldsymbol{L}_\partial = \frac{\partial \boldsymbol{\lambda}_{dq}}{\partial \boldsymbol{i}_{dq}} = \begin{bmatrix} l_d & l_{dq} \\ l_{dq} & l_q \end{bmatrix} \tag{2}$$

where l_d, l_q represents the incremental inductance along direct d and quadrature q-axis, respectively, while l_{dq} is the cross-saturation term. All quantities are functions of $\boldsymbol{i}_{dq}$. The stator flux linkage is expressed as

$$\boldsymbol{\lambda}_{dq} = \boldsymbol{L}(\boldsymbol{i}_{dq}) \cdot \boldsymbol{i}_{dq} + \boldsymbol{\lambda}_m = \begin{bmatrix} L_d & 0 \\ 0 & L_q \end{bmatrix} \cdot \boldsymbol{i}_{dq} + \begin{bmatrix} 0 \\ -\lambda_m \end{bmatrix} \tag{3}$$

where $\boldsymbol{L}$ is the apparent inductance matrix and λ_m is the open circuit permanent magnet flux linkage; $\lambda_m = 0$ corresponds to the SyR machine. The saturation and cross-saturation properities of the SyR machine under test is illustrated in the flux-map in Fig. 3 that is experimentally identified with constant speed test reported in [17].

The electromagnetic torque is given by

$$T = \frac{3p}{2}\,\boldsymbol{i}_{dq}^{\mathrm{T}}\,\mathbf{J}\,\boldsymbol{\lambda}_{dq} \tag{4}$$

where p is the number of pole pairs.

B. MTPA Law and Auxiliary-Flux Vector

Let γ denote the current angle according to the definition in Fig. 2. The change of torque with respect to the current angle

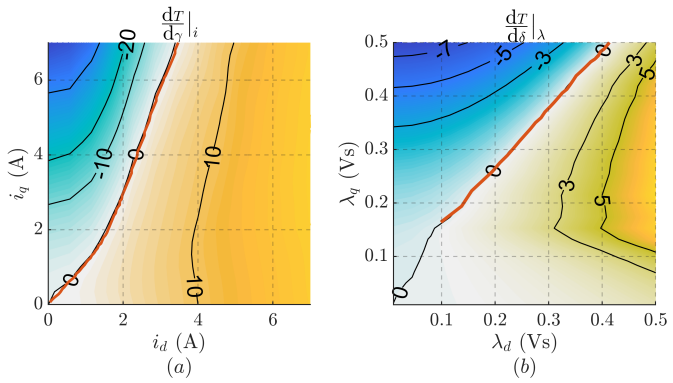

Fig. 4. Analytical evaluation of MTPA and MTPV laws for the SyR motor under test: (a) Contour of derivative of torque with respect to current angle (5) where the red line is the MTPA trajectory; (b) Contour of derivative of torque with respect to load angle (8) where the red line is the MTPV trajectory.

for a given current amplitude $i = |\boldsymbol{i}_{dq}|$ is computed as

$$\begin{aligned}\frac{\mathrm{d}T}{\mathrm{d}\gamma}\Big|_i &= \frac{3p}{2}\left(\frac{\mathrm{d}\boldsymbol{i}_{dq}^{\mathrm{T}}}{\mathrm{d}\gamma}\mathbf{J}\boldsymbol{\lambda}_{dq} + \boldsymbol{i}_{dq}^{\mathrm{T}}\mathbf{J}\frac{\mathrm{d}\boldsymbol{\lambda}_{dq}}{\mathrm{d}\gamma}\right)\\ &= \frac{3p}{2}\left(\boldsymbol{\lambda}_{dq}^{a}\right)^{\mathrm{T}}\mathbf{J}\boldsymbol{i}_{dq}\end{aligned} \tag{5}$$

where the auxiliary-flux vector $\boldsymbol{\lambda}_{dq}^{a}$ is defined as

$$\boldsymbol{\lambda}_{dq}^{a} = \mathbf{J}\boldsymbol{\lambda}_{dq} - \boldsymbol{L}_{\partial}\mathbf{J}\boldsymbol{i}_{dq}. \tag{6}$$

The MTPA trajectory is observed to be coincident with the zero locus of the contours of (5) in the dq current plane in Fig. 4(a) and is thus defined as

$$\frac{\mathrm{d}T}{\mathrm{d}\gamma}\Big|_i = 0 \implies \left(\boldsymbol{\lambda}_{dq}^{a}\right)^{\mathrm{T}}\mathbf{J}\boldsymbol{i}_{dq} = 0. \tag{7}$$

The expression (7) dictates that the MTPA criterion is respected *if and only if* the stator current is in phase with the auxiliary-flux vector, i.e., $\gamma_{\mathrm{MTPA}} = \angle\boldsymbol{\lambda}_{dq}^{a}$.

C. MTPV Law and Auxiliary-Current Vector

Let δ denote the load angle according to the definition in Fig. 2. Then, the change of torque with respect to load angle for a given flux amplitude $\lambda = |\boldsymbol{\lambda}_{dq}|$ is computed as

$$\begin{aligned}\frac{\mathrm{d}T}{\mathrm{d}\delta}\Big|_\lambda &= \frac{3p}{2}\left(\frac{\mathrm{d}\boldsymbol{i}_{dq}}{\mathrm{d}\delta}^{\mathrm{T}}\mathbf{J}\boldsymbol{\lambda}_{dq} + \boldsymbol{i}_{dq}^{\mathrm{T}}\mathbf{J}\frac{\mathrm{d}\boldsymbol{\lambda}_{dq}}{\mathrm{d}\delta}\right)\\ &= \frac{3p}{2}\boldsymbol{\lambda}_{dq}^{\mathrm{T}}\mathbf{J}\boldsymbol{i}_{dq}^{a}\end{aligned} \tag{8}$$

where the auxiliary-current vector $\boldsymbol{i}_{dq}^{a}$ is defined as

$$\boldsymbol{i}_{dq}^{a} = \mathbf{J}\boldsymbol{i}_{dq} - \boldsymbol{L}_{\partial}^{-1}\mathbf{J}\boldsymbol{\lambda}_{dq}. \tag{9}$$

The MTPV trajectory is observed to be coincident with the zero locus of the contours of (8) in the dq flux plane in Fig. 4(b) and is thus defined as

$$\frac{\mathrm{d}T}{\mathrm{d}\delta}\Big|_\lambda = 0 \implies \boldsymbol{\lambda}_{dq}^{\mathrm{T}}\mathbf{J}\boldsymbol{i}_{dq}^{a} = 0. \tag{10}$$

The expression (10) dictates that MTPV law is respected *if and only if* the auxiliary-current is in phase with the stator flux vector, i.e., $\delta_{\mathrm{MTPV}} = \angle\boldsymbol{i}_{dq}^{a}$.

III. Stator Flux Oriented Control

A. Stator Flux Oriented Reference

The stator flux oriented reference frame is denoted by subscript $f\tau$ where the stator flux linkage is aligned along f-axis and τ is the quadrature axis, i.e.,

$$\boldsymbol{\lambda}_{f\tau} = \begin{bmatrix}\lambda\\0\end{bmatrix} = \mathrm{e}^{-\delta\mathbf{J}}\boldsymbol{\lambda}_{dq}. \tag{11}$$

The voltage equation of a synchronous machine in the stator flux oriented reference frame is expressed as

$$\begin{bmatrix}s\lambda\\ \lambda\, s\delta\end{bmatrix} = \boldsymbol{v}_{f\tau} - R_s\,\boldsymbol{i}_{f\tau} - \omega\mathbf{J}\boldsymbol{\lambda}_{f\tau} \tag{12}$$

where the state variables are the stator flux magnitude and the load angle. The electromagnetic torque in the stator flux oriented reference frame simplifies to

$$T = \frac{3p}{2}\lambda\, i_\tau \tag{13}$$

where the controlled variables λ and i_τ are evidenced.

B. Modeling of Control Dynamics: State-of-Art

This section briefly recounts the state-of-art modelling of control dynamics reported in literature [13] [21]. The electromagnetic torque equation (4) in dq rotor reference frame can be reformulated using (3) as

$$T = \frac{3p}{2}\left(\frac{\lambda^2\sin(2\delta)}{2}\frac{L_d - L_q}{L_d\,L_q} + \lambda\,\cos(\delta)\,\frac{\lambda_m}{L_q}\right). \tag{14}$$

Equating (13) and (14), the torque producing current is

$$i_\tau = \frac{\lambda\sin(2\delta)}{2}\frac{L_d - L_q}{L_d\,L_q} + \cos(\delta)\,\frac{\lambda_m}{L_q}. \tag{15}$$

Previous models assume that the apparent inductances are constant and their derivative is thus negligible. Therefore, differentiating (15) gives

$$si_\tau = a'\cdot s\lambda + b'\cdot\lambda\, s\delta \tag{16}$$

where the terms a' and b' are

$$\begin{aligned}a' &= \frac{\sin(2\delta)}{2}\frac{L_d - L_q}{L_d\,L_q}\\ b' &= \cos(2\delta)\,\frac{L_d - L_q}{L_d\,L_q} - \frac{\sin(\delta)}{L_q}\,\frac{\lambda_m}{\lambda}.\end{aligned} \tag{17}$$

The cross-saturation effect is included in the apparent inductances, function of both current components. The assumption of constant apparent inductance in the differential equation (16) is inaccurate for machines with nonlinear magnetic model, as addressed in the following section.

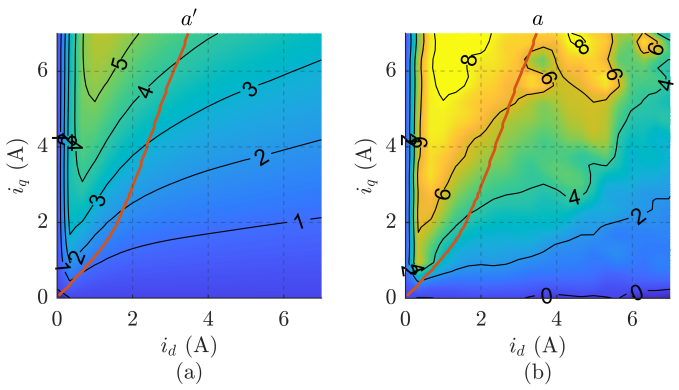

Fig. 5. Modeling discrepancy in the cross-coupling gain: (a) State-of-the-art a'; (b) Proposed a. Red line is the MTPA trajectory.

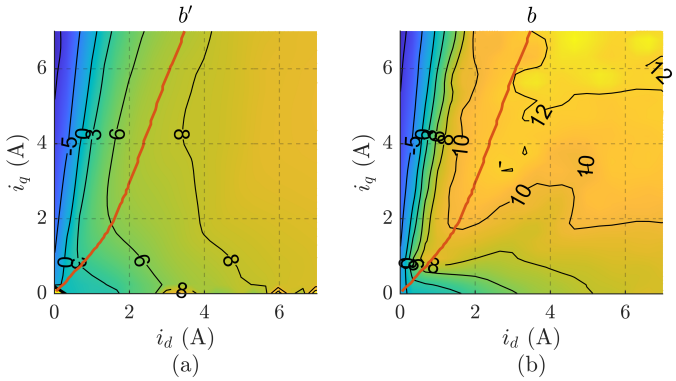

Fig. 6. Modeling discrepancy in the self-axis gain: (a) State-of-the-art b'; (b) Proposed b. Note that $b = 0$ contour is the MTPV trajectory. Red line is the MTPA trajectory.

C. Proposed Non-approximated Modeling

This section aims to build the dynamic model accounting for nonlinearity. The time-derivative of $\boldsymbol{\lambda}_{f\tau}$ in the stator flux reference frame is derived as

$$s\boldsymbol{\lambda}_{f\tau} = \begin{bmatrix} s\lambda \\ 0 \end{bmatrix} = s\left(\mathrm{e}^{-\mathbf{J}\delta}\,\boldsymbol{\lambda}_{dq}\right) = \mathrm{e}^{-\mathbf{J}\delta}\left[-\mathbf{J}\boldsymbol{\lambda}_{dq}\cdot s\delta + \boldsymbol{L}_{\partial}\cdot s\left(\mathrm{e}^{\mathbf{J}\delta}\,\boldsymbol{i}_{f\tau}\right)\right]. \tag{18}$$

Upon expanding the terms and rearranging leads to

$$\begin{bmatrix} s\lambda \\ 0 \end{bmatrix} = \mathrm{e}^{-\mathbf{J}\delta}\left(\boldsymbol{L}_{\partial}\mathbf{J}\,\boldsymbol{i}_{dq} - \mathbf{J}\boldsymbol{\lambda}_{dq}\right)\cdot s\delta + \mathrm{e}^{-\mathbf{J}\delta}\,\boldsymbol{L}_{\partial}\,\mathrm{e}^{\mathbf{J}\delta}\cdot\begin{bmatrix} si_f \\ si_\tau \end{bmatrix}. \tag{19}$$

Manipulating (19) using the auxiliary-current vector (9) and rearranging leads to

$$\begin{bmatrix} si_f \\ si_\tau \end{bmatrix} = \mathrm{e}^{-\mathbf{J}\delta}\,\boldsymbol{L}_{\partial}^{-1}\,\mathrm{e}^{\mathbf{J}\delta}\cdot\begin{bmatrix} s\lambda \\ 0 \end{bmatrix} + \frac{1}{\lambda}\begin{bmatrix} -\boldsymbol{\lambda}_{dq}^{\mathrm{T}}\,\boldsymbol{i}_{dq}^{a} \\ \boldsymbol{\lambda}_{dq}^{\mathrm{T}}\,\mathbf{J}\boldsymbol{i}_{dq}^{a} \end{bmatrix}\cdot s\delta \tag{20}$$

It follows from (20) that the dynamics of the controlled variables (λ, i_τ) are given by

$$\begin{bmatrix} s\lambda \\ si_\tau \end{bmatrix} = \begin{bmatrix} 1 & 0 \\ a & b \end{bmatrix}\begin{bmatrix} s\lambda \\ \lambda\, s\delta \end{bmatrix} \tag{21}$$

where the term a is the cross-coupling gain and the term b is the self-axis gain of the torque producing current loop. They are defined as

$$a = \frac{l_\Delta\,\sin(2\delta) - l_{dq}\,\cos(2\delta)}{l_d l_q - l_{dq}^2} \qquad b = \frac{1}{\lambda^2}\,\boldsymbol{\lambda}_{dq}^{\mathrm{T}}\,\mathbf{J}\,\boldsymbol{i}_{dq}^{a} \tag{22}$$

where $l_\Delta = (l_d - l_q)/2$ and $\boldsymbol{i}_{dq}^{a}$ is the auxiliary-current (9).

It is worth pointing out that the condition $b = 0$ corresponds to the MTPV law according to (10). It is of interest to represent the controlled variables (λ, i_τ) in terms of the state variables (λ, δ) in (12) as

$$\begin{bmatrix} s\lambda \\ \lambda\, s\delta \end{bmatrix} = \boldsymbol{T}\begin{bmatrix} s\lambda \\ s\,i_\tau \end{bmatrix} \qquad \boldsymbol{T} = \begin{bmatrix} 1 & 0 \\ -a/b & 1/b \end{bmatrix} \tag{23}$$

where $\boldsymbol{T}$ is the nonlinear transformation matrix.

The terms a and b are the counterparts of a' and b', respectively. The gains are dimensionally inverse of inductance (H^{-1}); thus, as apparent inductance is always greater than the incremental inductance due to saturation, the state-of-art gains (17) become underestimated. The significance of proposed approach is visualized by juxtaposing the terms a' and a in Fig. 5. The state-of-art approach underestimates this term up to a factor of 50%, especially at high load. For the data-point $i_d = 3$ A and $i_q = 6$ A on the MTPA trajectory, the cross-coupling gains are $a' = 4$ and $a = 6$.

Likewise, Fig. 6 reports the comparison of self-axis gains; the state-of-art approach b' is shown to underestimate b by a factor of approximately 50%.

IV. Direct Flux Vector Control

A. Hybrid Flux Observer

The observer is called hybrid to signify the combination of voltage and current models. Let $\boldsymbol{\Lambda}_{dq}$ denote the flux-map LUTs of the machine under test such that $\boldsymbol{\lambda}_{dq}^{i} = \boldsymbol{\Lambda}_{dq}(\boldsymbol{i}_{dq})$ where $\boldsymbol{\lambda}_{dq}^{i}$ denotes the current model flux estimate.

The flux observer is implemented in the stationary reference frame, defined as

$$s\hat{\boldsymbol{\lambda}}_{\alpha\beta} = \boldsymbol{v}_{\alpha\beta} - R_s\boldsymbol{i}_{\alpha\beta} + \mathrm{e}^{\mathbf{J}\theta}\,\boldsymbol{G}\left(\boldsymbol{\lambda}_{dq}^{i} - \hat{\boldsymbol{\lambda}}_{dq}\right) \tag{24}$$

where $\boldsymbol{G}$ is a 2×2 gain matrix. In this work, a diagonal matrix $\boldsymbol{G} = g\,\mathbf{I}$ is used. For electrical speeds above g rad/s, the voltage model (back-emf integration) prevails. The observed stator flux magnitude is $\hat{\lambda} = |\hat{\boldsymbol{\lambda}}_{dq}|$ and the observed load angle is $\hat{\delta} = \angle\hat{\boldsymbol{\lambda}}_{dq}$.

The incremental inductance matrix $\boldsymbol{L}_{\partial}$ is computed in real-time from the flux-map LUTs; as an example:

$$l_d(\boldsymbol{i}_{dq}) = \frac{\boldsymbol{\Lambda}_d(i_d + \delta i_d, i_q) - \boldsymbol{\Lambda}_d(i_d, i_q)}{\delta i_d} \tag{25}$$

where δi_d is a small value (≈ 10 mA). The other incremental inductances are computed in a similar fashion. Using the inductances, the gains (17) and (22) are estimated in real-time with the observed flux magnitude ($\delta \to \hat{\delta}$) and the observed load angle ($\lambda \to \hat{\lambda}$), represented as ($\hat{a}'$ & $\hat{b}'$) and ($\hat{a}$ & $\hat{b}$), respectively.

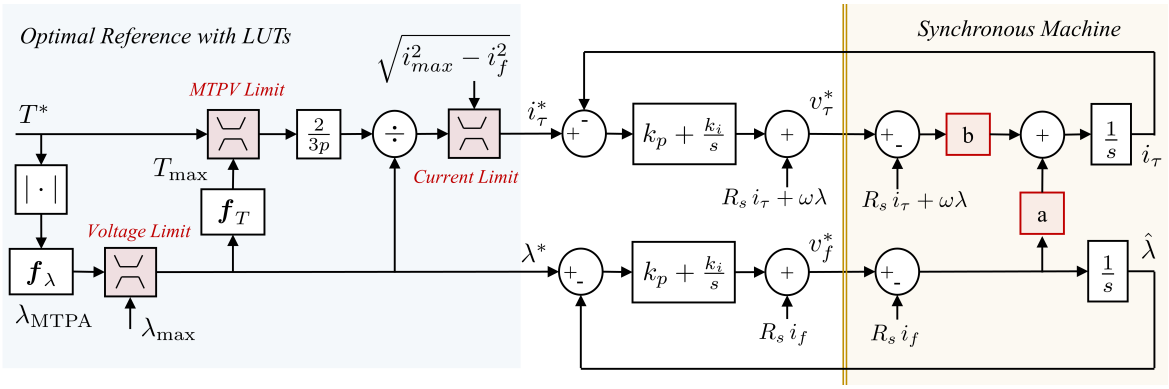

Fig. 7. Constant-gain PI DFVC control block diagram with the conventional LUT-based optimal reference. The closed loop of the linear regulators and the machine model is affected by the cross-coupling gain a and the self-axis gain b in the stator flux oriented reference frame.

B. Constant-Gain PI DFVC

For a PI stator flux oriented controller, the voltage reference is computed as

$$\boldsymbol{v}_{f\tau}^* = R_s\, \boldsymbol{i}_{f\tau} + \mathbf{J}\,\omega\,\boldsymbol{\lambda}_{f\tau} + \left[\boldsymbol{K}_p + \frac{\boldsymbol{K}_i}{s}\right] \begin{bmatrix} \lambda^* - \hat{\lambda} \\ i_\tau^* - i_\tau \end{bmatrix} \tag{26}$$

where the proportional $\boldsymbol{K}_p$ and integral $\boldsymbol{K}_i$ gains are constant diagonal matrices with terms k_{pf}, $k_{p\tau}$ and k_{if}, $k_{i\tau}$, respectively. The computation of the optimal references (λ^* & i_τ^*) is discussed in Section V.

The block diagram of the constant-gain PI DFVC is shown in Fig. 7, highlighting the linear regulator and the SyR machine model in stator flux oriented reference frame. It can be discerned from Fig. 7 that the τ-axis is coupled with f-axis through the cross-coupling gain a. Furthermore, the self-axis term b acts as a loop gain, making dynamics dependent on the operating point. To date, the constant-gain PI regulator implementation underestimated the bandwidth variability associated to the term b (was b'), as well as the weight of the cross-coupling term a (was a').

It is worth pointing out that the control approaches singularity at the MTPV limit ($b = 0$) which is an inherent limitation of the DFVC control.

C. Decoupled DFVC

Using (23), the voltage reference with decoupling transformation, shown in Fig. 8, is computed as

$$\boldsymbol{v}_{f\tau}^* = R_s\, \boldsymbol{i}_{f\tau} + \mathbf{J}\,\omega\,\boldsymbol{\lambda}_{f\tau} + \hat{\boldsymbol{T}} \left[\boldsymbol{K}_p + \frac{\boldsymbol{K}_i}{s}\right] \begin{bmatrix} \lambda^* - \hat{\lambda} \\ i_\tau^* - i_\tau \end{bmatrix} \tag{27}$$

where $\hat{\boldsymbol{T}}$ is the observed nonlinear transformation matrix (23) with the components $\hat{a}$ and $\hat{b}$.

The controller gains can be calibrated for a constant bandwidth in all operating points with $\boldsymbol{K}_p = k_p\,\mathbf{I}$ and $\boldsymbol{K}_i = k_i\,\mathbf{I}$ where the gains tuned for critical damping at $s = -\Omega$ are

$$k_p = 2\,\Omega \qquad k_i = \Omega^2. \tag{28}$$

The proposed decoupled scheme is similar to the one proposed in [13] using input-output feedback linearization, with the new contribution of the non-approximated evaluation of the transformation matrix $\boldsymbol{T}$.

V. Adaptive Reference Generation

A. Conventional LUTs-based Reference

The reference quantities are denoted with a superscript $*$. The optimal reference block diagram is shown in Fig. 7. The stator flux linkage for the reference torque at MTPA is computed as

$$\lambda_{\text{MTPA}} = \boldsymbol{f}_\lambda\big(|T^*|\big) \tag{29}$$

where $\boldsymbol{f}_\lambda$ is the MTPA LUT preprocessed offline using flux-map LUTs. The maximum stator flux linkage is a function of operating speed as

$$\lambda_{\max} = k_v\,\frac{v_{dc}}{\sqrt{3}\,\omega} \tag{30}$$

where k_v defines the voltage margin ($\approx$10%). Thus, the stator flux reference is obtained as $\lambda^* = \min\big(\lambda_{\text{MTPA}}, \lambda_{\max}\big)$.

The maximum torque $T_{\max}$ is a function of λ^*, determined by the MTPV limit $\boldsymbol{f}_T$ as

$$T_{\max} = k_T\,\boldsymbol{f}_T\big(\lambda^*\big) \tag{31}$$

where $\boldsymbol{f}_T$ is a MTPV LUT and k_T defines the torque margin. When the torque limit is in effect, $T_{\max}$ is relayed back to speed controller for anti-windup.

Note that DFVC approaches singularity at MTPV limit ($b = 0$); hence, a small margin ($\approx$ 10%) is necessary in implementation.

Finally, the reference torque producing current i_τ^* is calculated from T^* and λ^* using (13) and considering current limitation as shown in Fig. 7. Thus, the aforementioned choice of controlled variables (λ, i_τ) enables the DFVC to accommodate MTPA and flux-weakening operations with MTPV and current limits in a simple and straightforward fashion. This is a unique advantage over the commonly used CVC.

B. Online MTPA Adaptation

The block diagram of the proposed online LUT-less adaptive reference generation is shown in Fig. 8. To make the preprocessing of MTPA LUT obsolete, the flux adaptation for real-time MTPA tracking is designed from the analytical expression (7) as

$$\lambda_{\text{MTPA}} = \frac{k_A}{s}\,\big(\hat{\boldsymbol{\lambda}}_{dq}^{a}\big)^{\mathrm{T}}\,\mathbf{J}\,\boldsymbol{i}_{dq} \tag{32}$$

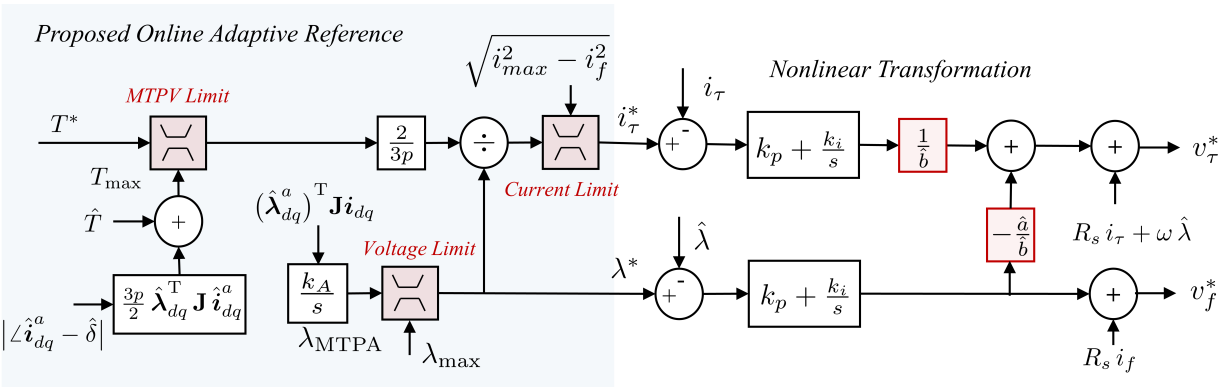

Fig. 8. Decoupled DFVC with the proposed online LUT-less adaptive reference generation and the nonlinear transformation matrix for constant bandwidth and uniform dynamic performance at all operating points.

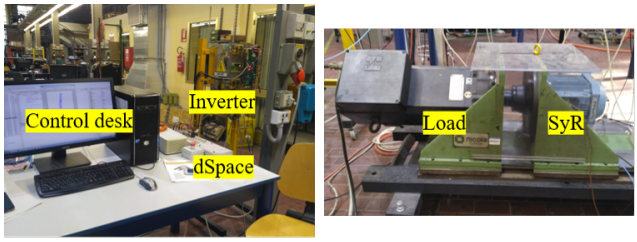

Fig. 9. Experimental Setup of 1.1 kW SyR motor under test on a dSPACE DS1103 control platform at a sampling frequency of 5 kHz.

where k_A is an integral gain to track the zero condition of crossproduct of the auxiliary-flux and the current vectors. The estimated auxiliary-flux vector $\hat{\boldsymbol{\lambda}}_{dq}^a$ is computed from the observed stator flux. The adaptation law ensures that the auxiliary-flux and the current vectors are in phase, and therefore respect the MTPA law 7. Note that the MTPA adaptation must be disabled in flux-weakening region to prevent the saturation of integrator in (32).

C. Online MTPV limit

Akin to the former section, the MTPV limit is real-time computed without dedicated LUTs using the analytical expression (10). As DFVC is unstable on the MTPV trajectory, an instantaneous hard constraint to limit torque is necessary.

The maximum permissible torque is computed from the estimated torque and load angle margin relating to the MTPV limit as

$$T_{\max} = k_T \left(|\hat{T}| + \left.\frac{\mathrm{d}T}{\mathrm{d}\delta}\right|_\lambda \cdot \left|\angle \hat{\boldsymbol{i}}_{dq}^a - \hat{\delta}\right| \right). \tag{33}$$

It follows from the derivative of torque with respect to δ (10) that

$$T_{\max} = k_T \left(|\hat{T}| + \frac{3p}{2}\, \hat{\boldsymbol{\lambda}}_{dq}^{\mathrm{T}} \mathbf{J}\, \hat{\boldsymbol{i}}_{dq}^a \cdot \left|\angle \hat{\boldsymbol{i}}_{dq}^a - \hat{\delta}\right| \right) \tag{34}$$

where $\hat{\boldsymbol{i}}_{dq}^a$ is the estimated auxiliary-current vector. Thus, the proposed adaptive torque limit in (34) makes the offline processing for MTPV LUTs obsolete.

TABLE I
MOTOR PARAMETERS

Parameters	Symbol	Values	Units
Rated power	P_n	1.1	kW
Rated voltage	V_n	340	V
Rated speed	ω_n	1500	rpm
Rated current	I_n	2.3	A
Rated torque	T_n	7.1	Nm
Pole pairs	p	2	-
Stator resistance	R_s	6.8	Ω
Shaft inertia	J	0.04	kgm^2

VI. EXPERIMENTAL RESULTS

The proposed decoupled DFVC is validated experimentally on a 1.1 kW SyR motor on a dSPACE DS1103 control platform running at a sampling frequency of 5 kHz. A picture of the setup is shown in Fig. 9. The parameters of the SyR motor under test are tabulated in Table I.

The flux observer gain is $g = 2\,\pi \cdot 5$ rad/s. The speed PI controller is tuned for critical damping at $s = -2\pi \cdot 1$ rad/s. The MTPA adaptive gain is $k_A = 60$.

A. Comparison with State-of-Art

To illustrate the significance of the proposed non-approximated dynamic model, the steady-state performance is evaluated at two different bandwidths of the stator flux regulators, $\Omega = 2\pi \cdot 100$ rad/s and $\Omega = 2\pi \cdot 200$ rad/s; the gains are tuned according to (28).

Figs. 10(a) and 10(b) report the torque control response of the decoupled DFVC at $\Omega = 2\pi \cdot 100$ rad/s for the state-of-art and the proposed non-approximated model, respectively where a similar steady-state response is observed. At time $t > 3$ s, the self-axis gain for the state-of-art model is underestimated by a factor $\hat{b}'/\hat{b} = 1.59$ which translates to the i_τ control loop pole positions $s = -2\pi \cdot 256$ rad/s and $s = -2\pi \cdot 62$ rad/s. However, this shift in poles due to under-compensation of the self-axis gain is not discernible in steady-state performance.

In Fig. 11(a) where the stator flux controller poles are designated for a higher bandwidth $\Omega = 2\pi \cdot 200$ rad/s. At time $t > 3$ s, the under-compensation of self-axis gain b

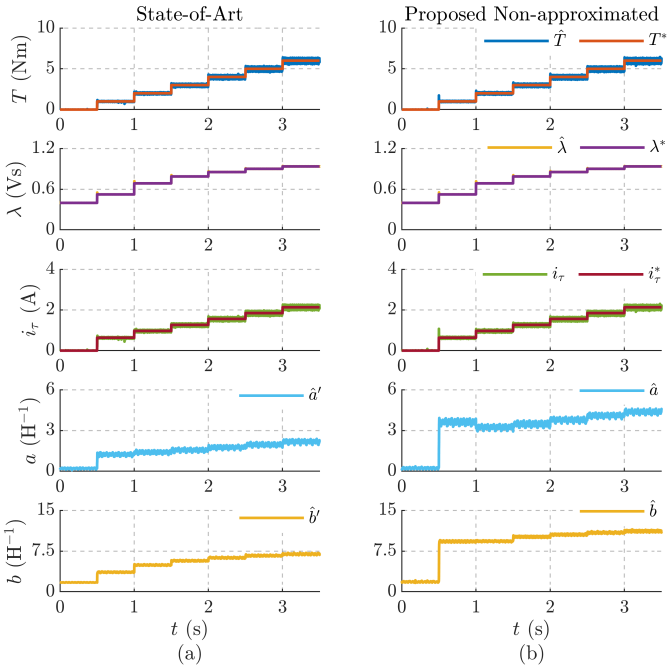

Fig. 10. Torque control at half rated speed, $\omega_r = 750$ rpm, using decoupled DFVC with the controller poles at $\Omega = 2\pi \cdot 100$ rad/s: (a) State-of-Art ($\hat{a}'$ & $\hat{b}'$); (b) Proposed Non-approximated ($\hat{a}$ & $\hat{b}$).

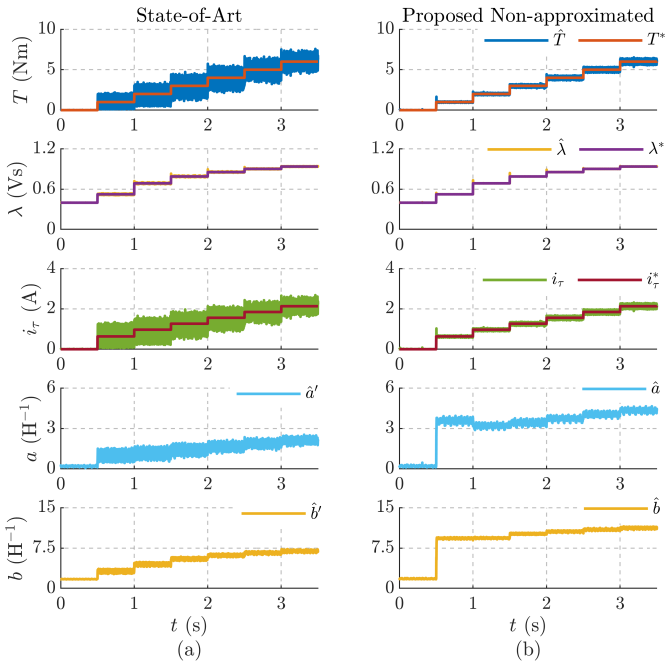

Fig. 11. Torque control at half rated speed, $\omega_r = 750$ rpm, using decoupled DFVC with the controller poles at $\Omega = 2\pi \cdot 200$ rad/s: (a) State-of-Art ($\hat{a}'$ & $\hat{b}'$); (b) Proposed Non-approximated ($\hat{a}$ & $\hat{b}$).

for the state-of-art model shifts the poles to $s = -2\pi \cdot 512$ rad/s and $s = -2\pi \cdot 124$ rad/s, resulting in a persistent high-frequency noise in the i_τ control loop. On the other hand, the proposed non-approximated in Fig. 11(b) has no high-frequency noise due to the precise compensation of the self-axis and cross-coupling gains. This results in a uniform and

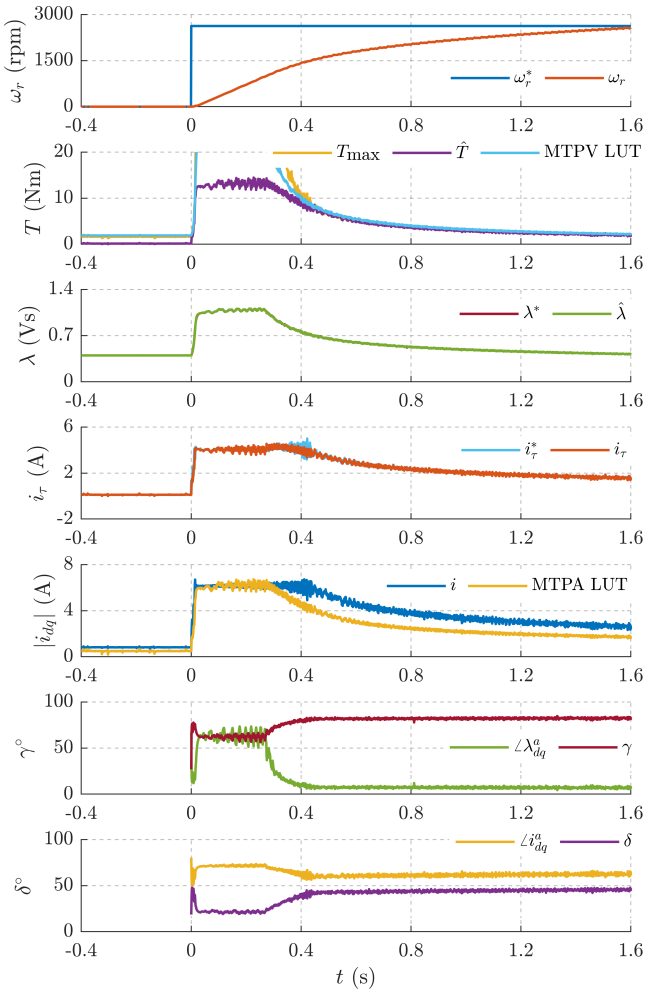

Fig. 12. Dynamic response of proposed DFVC with online adaptive reference for a speed step command $\omega_r^* = 0 \rightarrow 2625$ rpm (1.75 p.u) at $t = 0$ s.

stable performance at all operating points. Moreover, it is noteworthy to mention that the proposed method has similar execution time as that of the state-of-art method (≈ 42 μs).

B. Speed Control Response

The online adaptive reference scheme is validated with a speed control response at no load. In Fig. 12, a speed step reference $\omega_r^* = 0 \rightarrow 2625$ rpm (1.75 p.u) is commanded at $t = 0$ s.

1) MTPA Operation: The control operates at the current limit on MTPA for time $0 < t < 0.27$ s where the auxiliary-flux vector is observed to be in phase with the current vector. The maximum torque is constrained by the current limit, permitting 50% overload ($i_{\max} = 1.5\sqrt{2}\, I_n$). The MTPA LUT signal in Fig. 12 indicates the MTPA current amplitude corresponding to the present torque request, which is by definition incompatible with the voltage constraint when in flux weakening mode; it is discerned to be coincident with the current amplitude i, thus validating the adaptive flux controller.

2) Constant Current Locus: Due to the voltage limit, the control is prompted into flux-weakening at $t = 0.27$ s upon

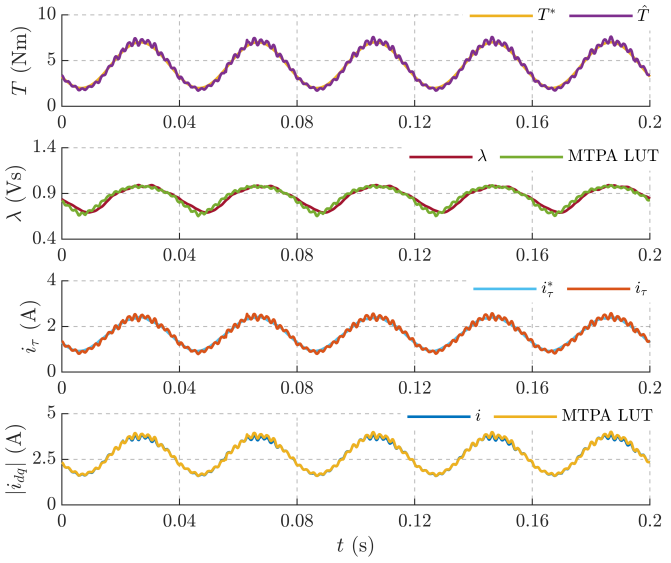

Fig. 13. Validation of adaptive flux reference for MTPA condition for a sinusoidal torque reference at 25 Hz at $\omega_r = 750$ rpm (0.5 p.u.).

which the optimal operating point traverses the locus of the maximum current limit for the time interval $0.27 < t < 0.45$ s.

3) MTPV Limit: For time $t > 0.45$ s, the torque is constrained by the MTPV limit $T_{\max}$ computed from (34). Note that the load angle and the phase of auxiliary-current vector do not converge due to the margin k_t necessary for stability. It can be observed that the estimated maximum torque $T_{\max}$ is coherent with the MTPV LUT values, thus validating the adaptive torque limit.

C. Adaptive Stator Flux for MTPA Tracking

The proposed stator flux adaptation for MTPA tracking in (32) is validated with a sinusoidal torque reference at 25 Hz in Fig. 13. It can be observed that the stator flux and the stator current magnitude are coincident with the values from the MTPA LUT, illustrating the feasibility of dynamic MTPA tracking.

D. Sensitivity Analysis to Parameter Error

The sensitivity to parameter errors is evaluated in Fig. 14 with a varying error in d-axis from -30% ($\hat{\lambda}^i_d = 1.3\,\lambda_d$) to +30% ($\hat{\lambda}^i_d = 0.7\,\lambda_d$) in steps of 10% increment every 0.5 s and a fixed error in q-axis of -25% ($\hat{\lambda}^i_q = 1.25\,\lambda_q$). The results correspond to operation at low speed of 300 rpm (0.2 p.u.) where the impact of the erroneous current-model flux-map on the flux observer is pronounced. The stator flux controller is tuned at $\Omega = 2\pi \cdot 150$ rad/s.

Fig. 14(a) shows the performance at rated torque with the state-of-art model; it is observed to suffer from high-frequency noise for the time $t > 2$ s as the self-axis gain is progressively under-compensated. At $t > 3$ s, the self-axis gain is under-compensated by a factor of $b/\hat{b}' = 3$ which translates to the pole positions $s = -2\pi \cdot 817$ rad/s and $s = -2\pi \cdot 82$ rad/s. The proposed non-approximated model in Fig. 14(b) is observed to

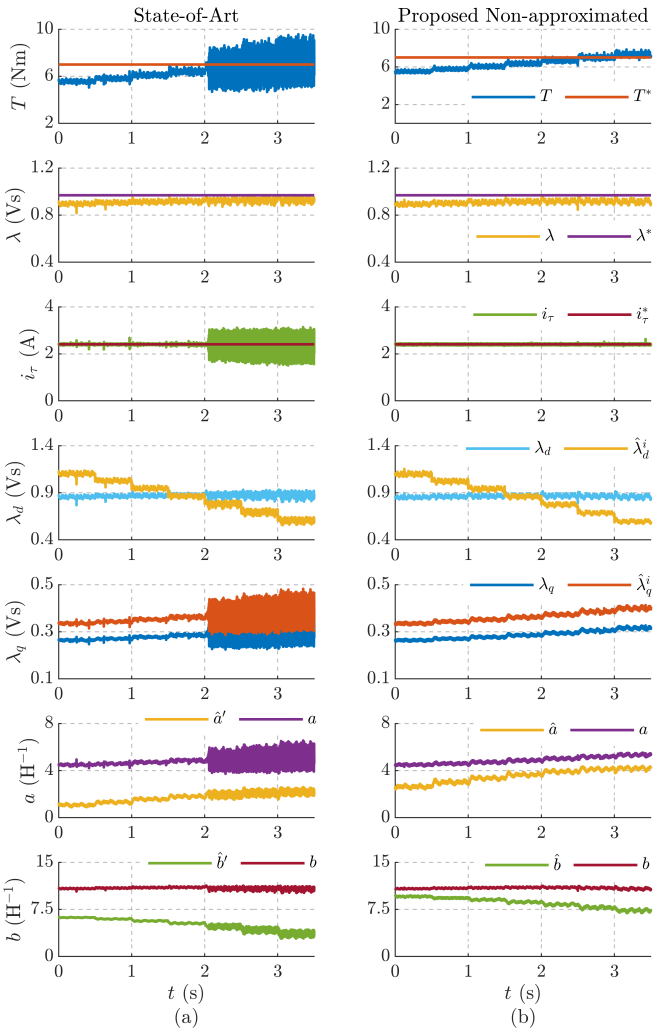

Fig. 14. Sensitivity analysis to parameter errors at $\omega_r = 300$ rpm (0.2 p.u.) and reference torque $T^* = 7.1$ Nm (1 p.u.): (a) State-of-art model; (b) Proposed non-approximated model. Varying error in d-axis from -30% to +30%, $\hat{\lambda}^i_d = 1.3\,\lambda_d \rightarrow \hat{\lambda}^i_d = 0.7\,\lambda_d$, in steps of 10% increment every 0.5 s; fixed error in q-axis, $\hat{\lambda}^i_q = 1.25\,\lambda_q$.

be more resilient as the under-compensation of the self-axis gain at $t > 3$ s is $b/\hat{b} = 1.5$, translating to the pole positions $s = -2\pi \cdot 354$ rad/s and $s = -2\pi \cdot 95$ rad/s. The non-ideal compensation of the cross-coupling gain a is observed to be less significant in steady-state conditions.

VII. Conclusion

This paper developed an accurate dynamic model accounting magnetic saturation of DFVC to expose the coupling between the f and the τ-axes. A nonlinear transformation matrix is proposed for decoupling in order to have a uniform bandwidth at all operating points. Through experimental evaluation, it is shown that, while the state-of-art model falters, the proposed non-approximated model is imperative for high bandwidth controllers. Moreover, the proposed model is shown to be more resilient under parameter detuning.

Furthermore, the auxiliary-flux and auxiliary-current vectors are defined to aid in online adaptation of MTPA and

MTPV criteria, respectively. The proposed adaptation schemes demonstrate the prospect of tracking both laws without the offline preprocessed LUTs. The feasibility and efficacy of the proposed schemes have been experimentally validated on a 1.1 kW SyR machine test bench.

REFERENCES

[1] S. Morimoto, Y. Takeda, T. Hirasa, and K. Taniguchi, "Expansion of Operating Limits for Permanent Magnet Motor by Current Vector Control Considering Inverter Capacity," *IEEE Transactions on Industry Applications*, vol. 26, DOI 10.1109/28.60058, no. 5, pp. 866–871, 1990.

[2] B. Cheng and T. R. Tesch, "Torque feedforward control technique for permanent-magnet synchronous motors," *IEEE Transactions on Industrial Electronics*, vol. 57, DOI 10.1109/TIE.2009.2038951, no. 3, pp. 969–974, 2010.

[3] H. A. A. Awan, Z. Song, S. E. Saarakkala, and M. Hinkkanen, "Optimal Torque Control of Saturated Synchronous Motors: Plug-and-Play Method," *IEEE Transactions on Industry Applications*, DOI 10.1109/TIA.2018.2862410, p. 1, 2018.

[4] J. M. Kim and S. K. Sul, "Speed control of interior permanent magnet synchronous motor drive for the flux weakening operation," *IEEE Transactions on Industry Applications*, vol. 33, DOI 10.1109/28.567075, no. 1, pp. 43–48, 1997.

[5] B. H. Bae, N. Patel, S. Schulz, and S. K. Sul, "New Field Weakening Technique for High Saliency Interior Permanent Magnet Motor," *Conference Record - IAS Annual Meeting (IEEE Industry Applications Society)*, vol. 2, no. 2, pp. 898–905, 2003.

[6] S. Bolognani, S. Calligaro, and R. Petrella, "Adaptive Flux-Weakening Controller for Interior Permanent Magnet Synchronous Motor Drives," *IEEE Journal of Emerging and Selected Topics in Power Electronics*, vol. 2, DOI 10.1109/JESTPE.2014.2299153, no. 2, pp. 236–248, 2014.

[7] Y. D. Yoon, W. J. Lee, and S. K. Sul, "New flux weakening control for high saliency interior permanent magnet synchronous machine without any tables," *2007 European Conference on Power Electronics and Applications, EPE*, DOI 10.1109/EPE.2007.4417350, 2007.

[8] M. F. Rahman, L. Zhong, and K. W. Lim, "A direct torque-controlled interior permanent magnet synchronous motor drive incorporating field weakening," *IEEE Transactions on Industry Applications*, vol. 34, DOI 10.1109/28.738985, no. 6, pp. 1246–1253, 1998.

[9] Y. Inoue, S. Morimoto, and M. Sanada, "Comparative study of PMSM drive systems based on current control and direct torque control in flux-weakening control region," *IEEE Transactions on Industry Applications*, vol. 48, DOI 10.1109/TIA.2012.2227134, no. 6, pp. 2382–2389, 2012.

[10] G. Pellegrino, E. Armando, and P. Guglielmi, "Direct flux field-oriented control of IPM drives with variable DC link in the field-weakening region," *IEEE Transactions on Industry Applications*, vol. 45, DOI 10.1109/TIA.2009.2027167, no. 5, pp. 1619–1627, 2009.

[11] G. Pellegrino, R. I. Bojoi, and P. Guglielmi, "Unified direct-flux vector control for AC motor drives," *IEEE Transactions on Industry Applications*, vol. 47, DOI 10.1109/TIA.2011.2161532, no. 5, pp. 2093–2102, 2011.

[12] G. Pellegrino, B. Boazzo, and T. M. Jahns, "Direct flux control of PM synchronous motor drives for traction applications," *2014 IEEE Transportation Electrification Conference and Expo: Components, Systems, and Power Electronics - From Technology to Business and Public Policy, ITEC 2014*, DOI 10.1109/ITEC.2014.6861836, no. c, pp. 1–6, 2014.

[13] H. A. A. Awan, M. Hinkkanen, R. Bojoi, and G. Pellegrino, "Stator-Flux-Oriented Control of Synchronous Motors: A Systematic Design Procedure," *IEEE Transactions on Industry Applications*, vol. 55, DOI 10.1109/TIA.2019.2927316, no. 5, pp. 4811–4820, 2019.

[14] B. Boazzo and G. Pellegrino, "Model-Based Direct Flux Vector Control of Permanent-Magnet Synchronous Motor Drives," *IEEE Transactions on Industry Applications*, vol. 51, DOI 10.1109/TIA.2015.2399619, no. 4, pp. 3126–3136, 2015.

[15] S. Rubino, I. R. Bojoi, E. Armando, and A. Tenconi, "Deadbeat Direct Flux Vector Control of Surface Permanent Magnet Motor Drives," *IEEE Transactions on Industry Applications*, vol. 56, DOI 10.1109/TIA.2020.2972835, no. 3, pp. 2685–2699, 2020.

[16] X. Lin, W. Huang, W. Jiang, Y. Zhao, and S. Zhu, "Deadbeat Direct Torque and Flux Control for Permanent Magnet Synchronous Motor Based on Stator Flux Oriented," *IEEE Transactions on Power Electronics*, vol. 35, DOI 10.1109/TPEL.2019.2946738, no. 5, pp. 5078–5092, 2020.

[17] E. Armando, R. I. Bojoi, P. Guglielmi, G. Pellegrino, and M. Pastorelli, "Experimental identification of the magnetic model of synchronous machines," *IEEE Transactions on Industry Applications*, vol. 49, DOI 10.1109/TIA.2013.2258876, no. 5, pp. 2116–2125, 2013.

[18] M. Hinkkanen, P. Pescetto, E. Mölsä, S. E. Saarakkala, G. Pellegrino, and R. Bojoi, "Sensorless Self-Commissioning of Synchronous Reluctance Motors at Standstill Without Rotor Locking," *IEEE Transactions on Industry Applications*, vol. 53, DOI 10.1109/TIA.2016.2644624, no. 3, pp. 2120–2129, 2017.

[19] P. Pescetto and G. Pellegrino, "Automatic Tuning for Sensorless Commissioning of Synchronous Reluctance Machines Augmented with High-Frequency Voltage Injection," *IEEE Transactions on Industry Applications*, vol. 54, DOI 10.1109/TIA.2018.2839600, no. 5, pp. 4485–4493, 2018.

[20] A. Varatharajan, P. Pescetto, and G. Pellegrino, "Sensorless Self-Commissioning of Synchronous Reluctance Machine with Rotor Self-Locking Mechanism," in *2019 IEEE Energy Conversion Congress and Exposition (ECCE)*, DOI 10.1109/ECCE.2019.8913023, pp. 812–817, 2019.

[21] A. Yousefi-Talouki, P. Pescetto, and G. Pellegrino, "Sensorless Direct Flux Vector Control of Synchronous Reluctance Motors Including Standstill, MTPA, and Flux Weakening," *IEEE Transactions on Industry Applications*, vol. 53, DOI 10.1109/TIA.2017.2679689, no. 4, pp. 3598–3608, 2017.

Anantaram Varatharajan (S'18) received his B.E.(Honours) degree in Electrical and Electronics engineering from BITS Pilani University, India in 2013 and M.Sc. degree in Sustainable Transportation and Electrical Power Systems (STEPS), an Erasmus Mundus Master Program from University of Oviedo, Spain, in 2016. Since 2017, he is a doctoral student at the department of energy, Politecnico di Torino, Turin, Italy.

His research interests include sensorless and advanced control of synchronous motor drives.

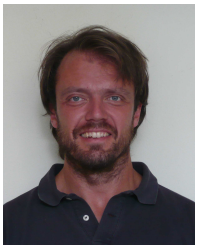

Gianmario Pellegrino (M'06-SM'13) received the MSc and PhD degrees in electrical engineering from Politecnico di Torino, Turin, Italy in 1998 and 2002, respectively. He is currently a Professor of Electrical Machines and Drives at the same university.

He is engaged in several research projects with the industry, and one of the authors of the open-source project SyR-e for the design of electrical motors. He was a visiting fellow at Aalborg University, Denmark, the University of Nottingham, UK, and the University of Wisconsin-Madison, USA. Dr. Pellegrino is an Associate Editor for the IEEE Transactions on Industry Applications and an IEEE Senior Member. He has 50 IEEE journal papers, two patents and seven Best Paper Awards.

Dr. Pellegrino is a member of the Power Electronics Interdepartmental Laboratory (PEIC) established in 2017 at the Politecnico di Torino and a member of the Advisory Board of PCIM (Power Conversion and Intelligent Motion) Europe. He is currently the Vice President of the CMAEL (Convertitori, Macchine e Azionamenti Elettrici) Association, representative of the scholars in Power Converters, Electrical Machines and Drives in Italy, and the Rector's Advisor for Interdepartmental Centres of Politecnico di Torino.

Eric Armando (M'15-SM'19) received the M.Sc. and Ph.D. degrees in electrical engineering from Politecnico di Torino, Turin, Italy, in 2002 and 2008, respectively. He is now with Politecnico di Torino as Associate Professor of Power Converters, Electrical Machines and Drives.

His fields of interest are power electronics and high-performance AC motor drives. Prof. Armando is co-author of numerous Journal Papers and of three Patents. Over the years he received three awards for innovation and one paper award from the Power Electronics Technical Committee of the IEEE Industrial Electronics Society.